PNAS

Supporting Information for

Entropic control of the free energy landscape of an archetypal biomolecular machine

Korak Kumar Ray[1], Colin D. Kinz-Thompson[1,†], Jingyi Fei[1,‡], Bin Wang[2,§], Qiao Lin[2], Ruben L. Gonzalez Jr[1,*]

[1]Department of Chemistry, Columbia University, New York, NY 10027 USA

[2]Department of Mechanical Engineering, Columbia University, New York, NY 10027 USA

[†]Present address: Department of Chemistry, Rutgers University-Newark, Newark, NJ 07102 USA

[‡]Present address: Department of Biochemistry and Molecular Biology, University of Chicago, Chicago, IL 60637 USA

[§]Present address: Becton, Dickinson, and Company, Brea, California 92821 USA

***Corresponding Author**: Ruben L. Gonzalez, Jr., Department of Chemistry, Columbia University, 3000 Broadway, New York, NY, 10027, USA, Tel: (212) 854-1096; FAX: (212) 932-1289; **Email:** rlg2118@columbia.edu

This PDF file includes:

Figures S1 to S5
Tables S1 to S3

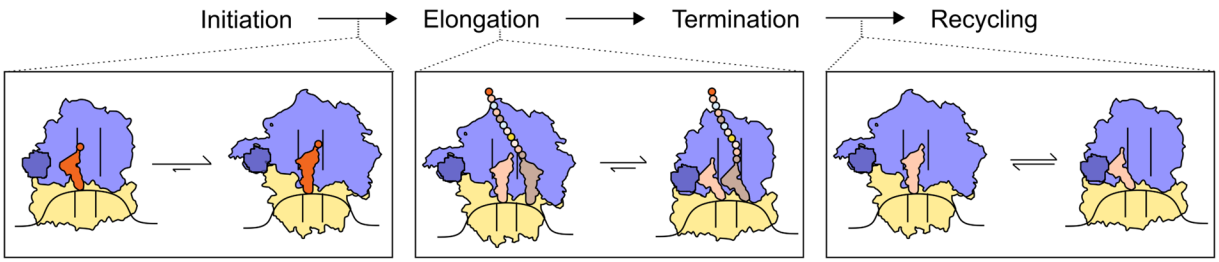

Figure S1. GS1 ⇌ GS2 or analogous equilibria in the translation pathway. Schematic of the four major stages of ribosome-catalyzed protein synthesis (top) and the role that regulation of the GS1⇌GS2 equilibrium (or analogous equilibria between RC global states similar to GS1 and GS2) plays along this reaction pathway (bottom).

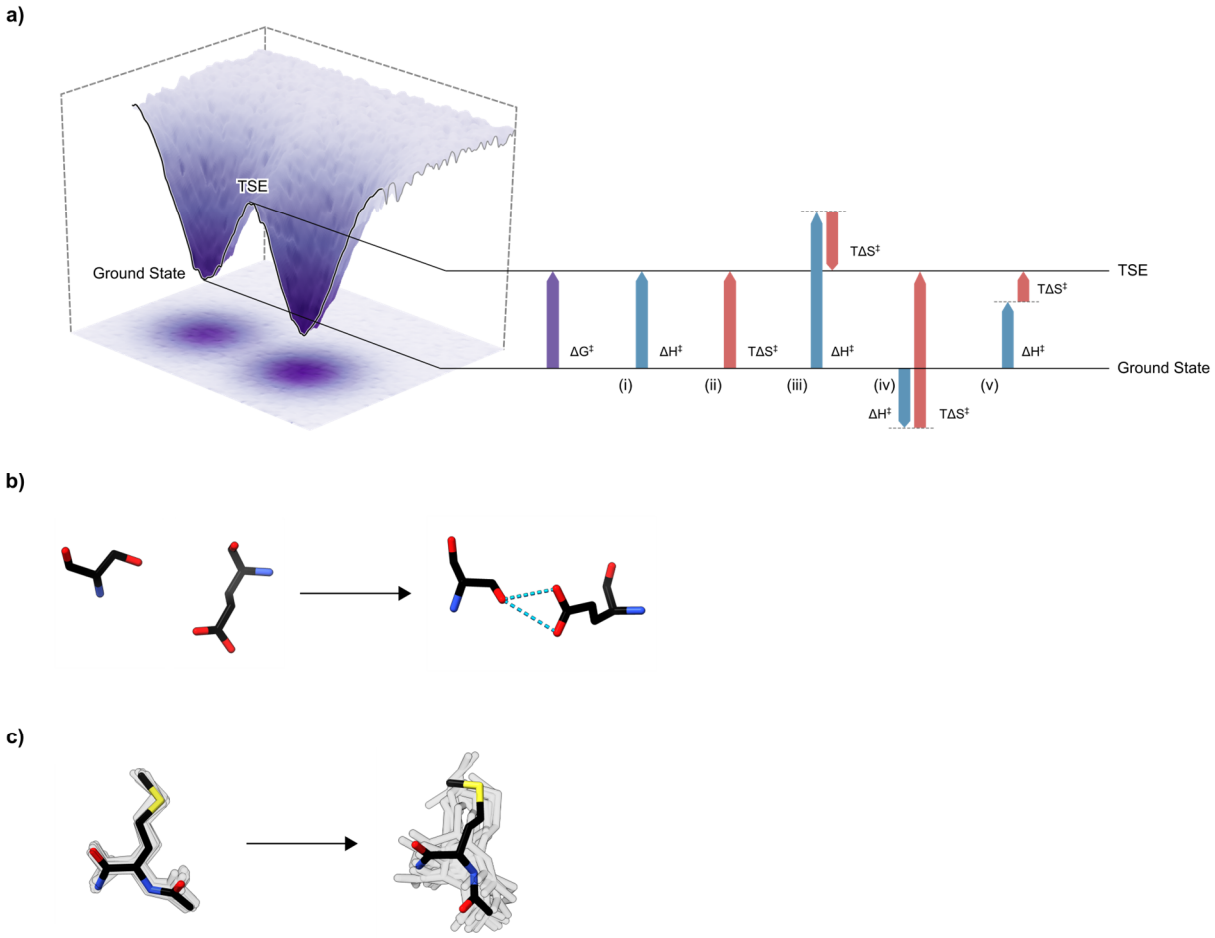

Figure S2. Free energy landscapes and their mechanistic implications (**a**) A hypothetical free energy ($\Delta G^{\ddagger}$) (purple) barrier and the combinations of enthalpic ($\Delta H^{\ddagger}$) (blue) and entropic ($\Delta S^{\ddagger}$) (red) components capable of comprising that barrier. Specifically, the barrier may be comprised of components that are (i) purely enthalpically unfavorable (ii) purely entropically unfavorable, (iii) enthalpically unfavorable-entropically favorable, (iv) enthalpically favorable-entropically unfavorable, or (v) enthalpically unfavorable-entropically unfavorable. In cases iii-v, the dotted line shows the height of the barrier if enthalpy was the only contributing component. Because the enthalpic component reports on remodeling of inter- and intramolecular interactions, and the entropic component reports on changes in the number of microstates (interpreted as modulating structural flexibility of the system) during the transition, each of i-v shows a different structural and physical mechanism underlying the same free energy barrier. **(b-c)** Representative structural interpretations of **(b)** enthalpically and **(c)** entropically favorable processes. The enthalpically favorable process leads to the formation of intermolecular interactions (in this case, hydrogen bonds) between the depicted serine and glutamate residues. The entropically favorable process leads to an increase in the number of microstates (in this case, conformational rotamers) of the depicted methionine residue, thereby making it more flexible. For completeness, we note that the reverse processes (i.e., breaking of the hydrogen bonds between the serine and glutamate residues and a decrease in the number of conformational rotamers of the methionine) would constitute **(b)** enthalpically and **(c)** entropically unfavorable processes.

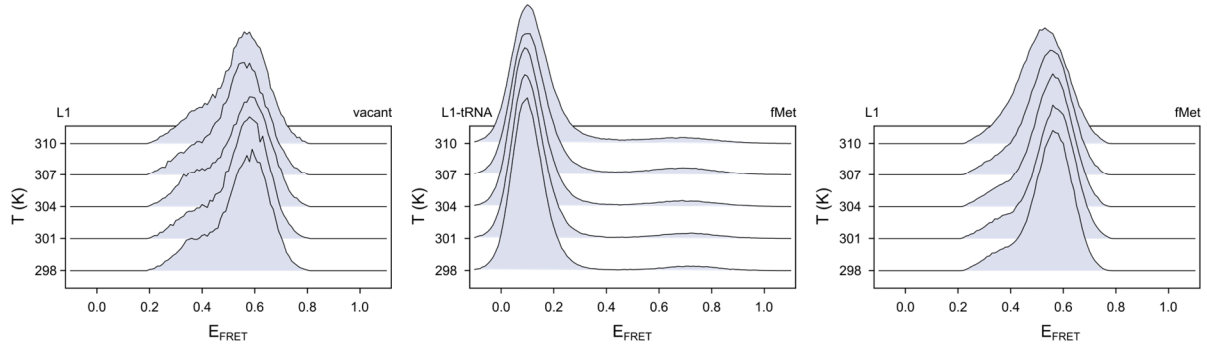

Figure S3. Histograms of smFRET signals for various RCs. Histograms of E_{FRET} values collected using $smFRET_{L1}$ for RC^{vacant} (left), $smFRET_{L1\text{-}tRNA}$ for RC^{fMet} (center), and $smFRET_{L1}$ for RC^{fMet} (right) at five temperature points between 298 K and 310 K.

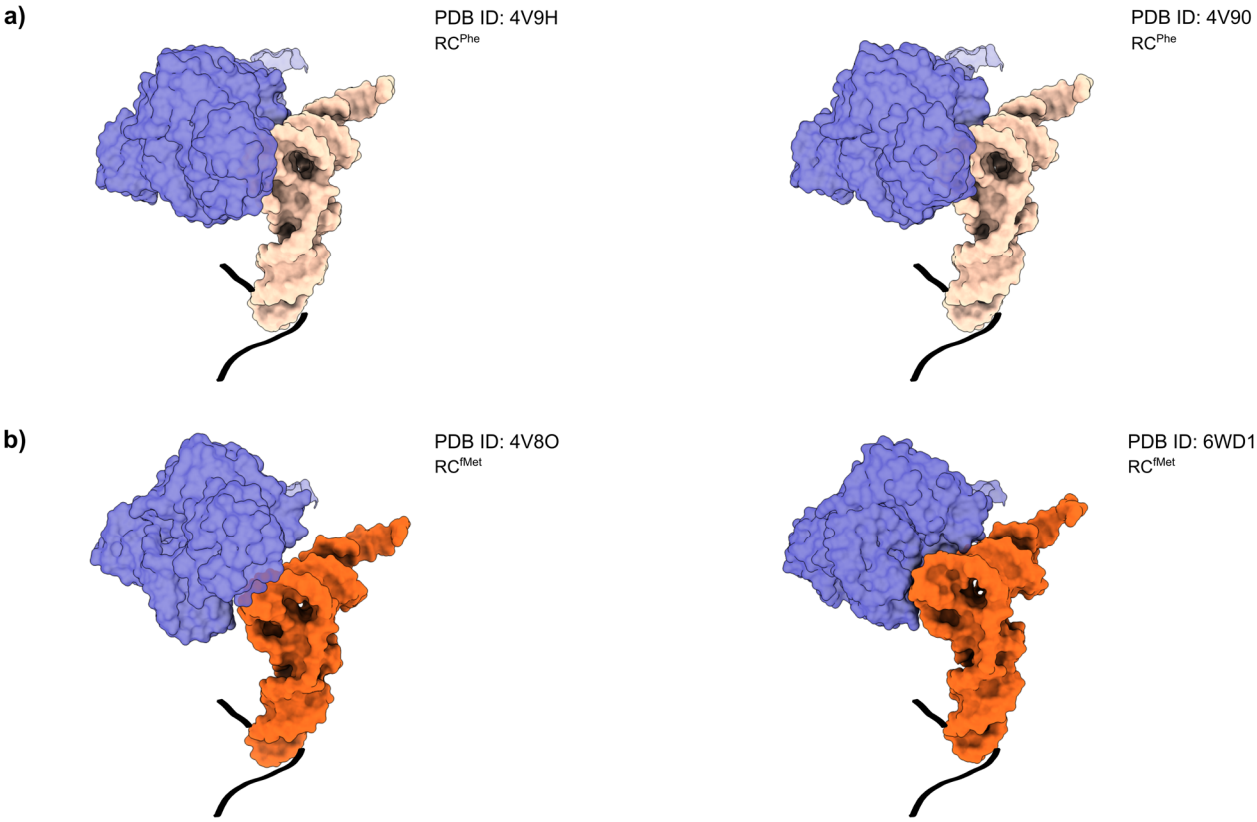

Figure S4. The conformations of the tRNA and L1 stalk in GS2-like conformations for RC^{Phe} and RC^{fMet}. (a) The atomic structures of GS2-like conformations from RCs analogous to RC^{Phe} are compared to **(b)** the atomic structures of GS2-like conformations from RCs analogous to RC^{fMet}. The four structures were positioned in the same orientation by aligning the anticodon stem loops of the tRNAs, were rendered in surface representations, and, for clarity, only the L1 stalk (the entire uL1 protein and nucleotides 2100-2200 of the 23S rRNA) (dark purple), tRNAs (tan for $tRNA^{Phe}$ or orange for $tRNA^{fMet}$), and path of the mRNA (black) are displayed.

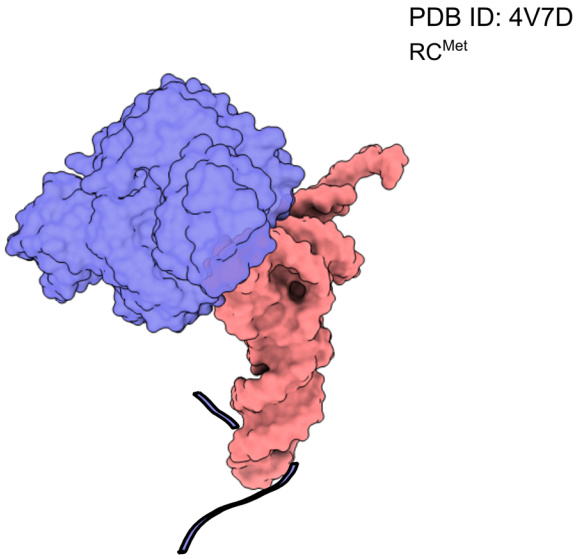

Figure S5. The conformation of the tRNA and L1 stalk in a GS2-like conformation for RC^{fMet}. Reconstructed atomic structure of an RC analogous to RC^{Met} in a GS2-like conformation. While the RC had been prepared using tRNA^{Met}, the original structural model had been constructed using tRNA^{Phe}. In this model, the tRNA has been replaced with tRNA^{Met}, with a further round of rigid body refinement. The RC is positioned to the same orientation as the previous RCs (in Extended Data Figure 4) utilizing the alignment of the anticodon stem loops of the tRNAs. Similar to the previous structures, this structure was rendered in surface representation and, for clarity, only the L1 stalk (the entire uL1 protein and nucleotides 2100-2200 of the 23S rRNA) (dark purple), tRNA^{Met} (pink), and path of the mRNA (black) are displayed.

Table S1. The number of smFRET trajectories and total number of datapoints (in parentheses) used for analysis for each RC at each temperature.

	Trajectories (Datapoints)				
	298 K	301 K	304 K	307 K	310 K
RC^{vacant}	340 (32321)	296 (25829)	363 (34887)	369 (31874)	366 (31958)
RC^{Phe} (L1)	590 (64281)	536 (68000)	543 (72474)	542 (68879)	387 (46057)
RC^{Phe} (L1-tRNA)	407 (111307)	420 (128693)	467 (151071)	452 (128637)	361 (105157)
RC^{fMet} (L1)	1769 (219410)	1485 (183364)	1540 (181060)	1804 (191044)	1739 (158692)
RC^{fMet} (L1-tRNA)	752 (294998)	725 (334850)	787 (287819)	954 (334174)	897 (306594)

Table S2. Activation parameter values for all RCs. The absolute values of activation parameters for each RC. Errors are standard deviations of the marginalized posterior probability distributions of each parameter (see Methods, and Table S1 for the number of individual molecules per dataset).

	GS1→GS2		GS2→GS1	
	$\Delta H^{\ddagger}$ (kcal mol^{-1})	$\Delta S^{\ddagger}$ (cal K^{-1} mol^{-1})	$\Delta H^{\ddagger}$ (kcal mol^{-1})	$\Delta S^{\ddagger}$ (cal K^{-1} mol^{-1})
RC^{vacant}	13 ± 1	−16 ± 3	9.4 ± 0.9	−23 ± 3
RC^{Phe} (L1)	40 ± 2	75 ± 5	34 ± 2	54 ± 5
RC^{Phe} (L1-tRNA)	40.8 ± 0.4	77 ± 1	34.1 ± 0.4	56 ± 1
RC^{fMet} (L1)	21.5 ± 0.3	15.0 ± 0.9	10.2 ± 0.2	−19.4 ± 0.8
RC^{fMet} (L1-tRNA)	21.2 ± 0.2	12.0 ± 0.6	10.4 ± 0.2	−18.4 ± 0.6

Table S3. The prior probability distributions used for the parameters during the global BIASD analysis. ϵ_{GS1} and ϵ_{GS2} are the mean E_{FRET}s for GS1 and GS2 respectively; σ is the noise for both states; $\Delta H^{\ddagger}_{(GS1\rightarrow GS2)}$ and $\Delta H^{\ddagger}_{(GS2\rightarrow GS1)}$ are the enthalpic components of the free energy barriers for the GS1→GS2 and GS2→GS1 transitions respectively; and $\Delta S^{\ddagger}_{(GS1\rightarrow GS2)}$ and $\Delta S^{\ddagger}_{(GS2\rightarrow GS1)}$ are the corresponding entropic components. μ and τ are the mean and standard deviations of the Gaussian distribution, while a and b are the minimum and maximum values of the uniform distribution.

Parameter	Dataset	Distribution	Distribution Parameters
ϵ_{GS1}	$smFRET_{L1\text{-}tRNA}$	Gaussian	μ = 0.15, τ = 0.1
	$smFRET_{L1}$ (RC^{Phe})	Gaussian	μ = 0.55, τ = 0.1
	$smFRET_{L1}$ (RC^{vacant} and RC^{fMet})	Gaussian	μ = 0.5840, τ = 0.0001
ϵ_{GS2}	$smFRET_{L1\text{-}tRNA}$	Gaussian	μ = 0.85, τ = 0.1
	$smFRET_{L1}$ (RC^{Phe})	Gaussian	μ = 0.35, τ = 0.1
	$smFRET_{L1}$ (RC^{vacant} and RC^{fMet})	Gaussian	μ = 0.3545, τ = 0.0001
σ	All	Uniform	a = 0.0001, b = 0.15
$\Delta H^{\ddagger}_{(GS1\rightarrow GS2)}$	All	Uniform	$a = -5 \times 10^5$, $b = 5 \times 10^5$
$\Delta S^{\ddagger}_{(GS1\rightarrow GS2)}$	All	Uniform	a = −1000, b = 1000
$\Delta H^{\ddagger}_{(GS2\rightarrow GS1)}$	All	Uniform	$a = -5 \times 10^5$, $b = 5 \times 10^5$
$\Delta S^{\ddagger}_{(GS2\rightarrow GS1)}$	All	Uniform	a = −1000, b = 1000